

## Experimental Realization of a Colloidal Ratchet Effect in a non-Newtonian Fluid


Guillermo Camacho<sup>1</sup>,<sup>1</sup> Alejandro Rodriguez-Barroso<sup>1</sup>,<sup>1</sup> Oscar Martinez-Cano,<sup>1</sup> Jose R. Morillas<sup>1</sup>,<sup>1</sup> Pietro Tierno<sup>2,3,4,\*</sup> and Juan de Vicente<sup>1</sup>

<sup>1</sup>*F2N2Lab, Magnetic Soft Matter Group and Excellence Research Unit 'Modeling Nature' (MNat), Department of Applied Physics, Faculty of Sciences, University of Granada, C/Fuentenueva s/n, Granada 18071, Spain*

<sup>2</sup>*Departament de Física de la Matèria Condensada, Universitat de Barcelona, Barcelona 08028, Spain*

<sup>3</sup>*Institut de Nanociència i Nanotecnologia, Universitat de Barcelona, Barcelona 08028, Spain*

<sup>4</sup>*Universitat de Barcelona Institute of Complex Systems (UBICS), Universitat de Barcelona, Barcelona 08028, Spain*

 (Received 20 July 2022; revised 10 January 2023; accepted 30 January 2023; published 21 February 2023)

Shear thinning fluids represent a class of non-Newtonian media characterized by a decrease of the apparent viscosity when increasing the shear rate. Here we experimentally demonstrate a deterministic ratchet effect in such media that enables directed transport of microscopic particles under a square-wave magnetic force. The applied modulation is designed in such a way that it does not produce any average speed when the particles are dispersed in a Newtonian fluid (e.g., water). However, in a dilute biopolymer solution, we observe the emergence of a net colloidal current when the forcing wave is composed of different amplitudes and time durations within a single period. The shear thinning nature of the dispersing medium nonlinearly raises the mean speed for strong forces, breaking the spatial symmetry of the particle displacement and generating a net colloidal transport. We complement our findings with numerical simulations that capture well the underlying physical mechanism, showing good agreement with the experimental results. Our technique to ratchet magnetic particles could be potentially extended in active microrheology to probe other non-Newtonian, complex fluids and to infer the nonlinear properties of viscoelastic materials.

DOI: [10.1103/PhysRevApplied.19.L021001](https://doi.org/10.1103/PhysRevApplied.19.L021001)

Since the pioneering lecture of Richard Feynman [1], the transport of matter with a ratchet effect has fascinated scientists for a long time [2,3]. From the fundamental side, any generic ratchet mechanism makes use of spatial or temporal asymmetries to convert external fluctuations into directed motion and takes place in several biological and physical processes. Such processes range from the translocation of proteins [4], molecular motors [5–7] or enzymes [8] to information [9–11] and financial [12–14] systems. On the application side, the ratchet effect represents a convenient way to extract useful work from a thermodynamic system, and different schemes have been proposed in a variety of systems, from dusty plasma [15] to nanoparticles [16,17], artificial spin ice [18,19], domain walls [20,21], vortices in high- $T_c$  superconductors [22–24], or active matter [25–28], to cite only a few of them.

Different works based on the use of fixed or time-dependent external potentials, have shown that microscopic colloidal particles can be used as an experimentally accessible model system to investigate ratchet transport effects [29–34]. Moreover, these efforts have

inspired further theoretical works aimed at proposing more efficient transport schemes for other condensed matter systems. However, most of the mechanisms proposed so far concern the use of a Newtonian fluid as a carrier, i.e., characterized by a constant viscosity when varying the shear rate. Thus, in such systems a linear relationship between the applied force and the resulting velocity governs the particle dynamics and determines the basic mechanism of particle motion. While active particles in viscoelastic media have recently become the matter of interest [35–37], experiments on ratchet effects in non-Newtonian media are scarce or relegated to theoretical propositions [38–42]. Moreover, the subject of transport via the ratchet effect in viscoelastic media leads subsequently to different developments in the field of molecular motors and anomalous versus normal cargo transport [43–47].

Here we provide such an experimental realization and demonstrate that, under a periodic square-wave forcing of different plateaus, which produces no net particle movement in a Newtonian liquid (e.g., water), the shear thinning nature of the dispersing medium generates an asymmetry in speed, which triggers a biased particle transport. We characterize the mean particle speed by varying the different field parameters, and further develop a numerical

\*ptierno@ub.edu

simulation code that can explain the observed results by balancing the magnetophoretic force with the viscous one arising from the particle motion. Thus, we provide a technique to steer microscopic magnetic particles via a square-wave modulation, which represents a versatile and powerful way to programmably transport magnetic colloidal matter in complex media including those that are biological.

A power-law fluid is usually characterized by a relatively large apparent viscosity when compared to that of water. Thus, we have build up a special set of magnetic coils capable of generating large enough magnetic field gradients to transport dispersed particles, as shown in the top inset in Fig. 1(a); further experimental details

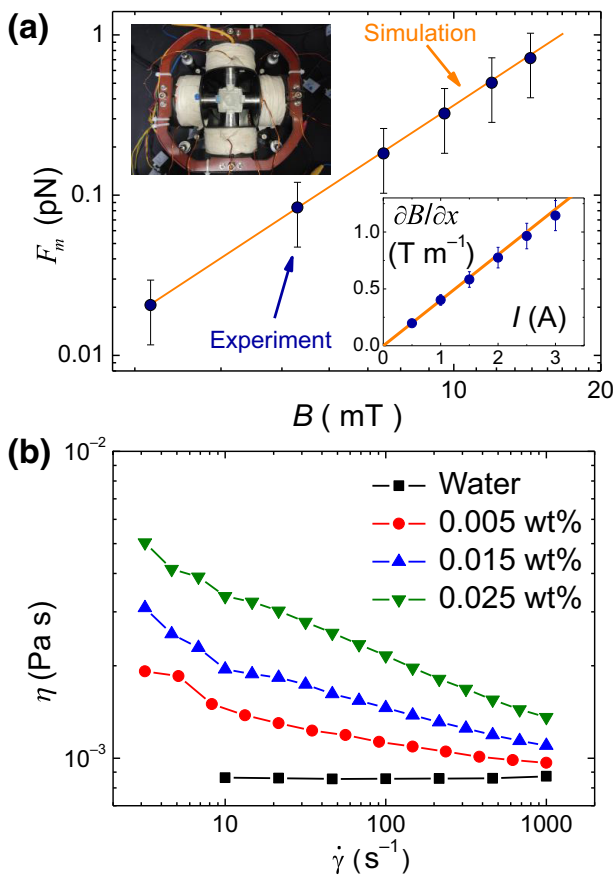


FIG. 1. (a) Double logarithmic plot of the magnetophoretic force  $F_m$  versus magnetic field density  $B$  showing the quadratic dependence  $F_m \sim B^2$ . The top inset shows an image of the experimental system. The bottom inset displays the corresponding magnetic field gradient  $\partial B/\partial x$  versus the current  $I$  circulating in the coil system. In both graphs, filled points are experimental data while continuous lines correspond to finite-element simulations. (b) Shear viscosity  $\eta$  versus shear rate  $\dot{\gamma}$  for different concentrations of Xanthan gum in water. The corresponding scaling indexes are  $n = 0.88$  (0.005 wt% of Xanthan gum),  $n = 0.85$  (0.015 wt%), and  $n = 0.76$  (0.025 wt%).

including a scheme of the setup are given in the Supplemental Material [48], which includes Refs. [49–51]. The coils are made of 612 turns of copper wire and feature cylindrical cores of mu-metal. They are able to generate a uniform magnetic field density up to  $B = 16$  mT and a spatial gradient up to  $\partial B/\partial x = 1.2$  T m $^{-1}$ , as shown in the bottom inset in Fig. 1(a). The spatial uniformity of the field in the sample plane is characterized with a teslameter and confirmed by the numerical finite-element method (COMSOL simulations). As shown in Fig. 1(a), the results of such a numerical study agree quantitatively well with the measured field gradient. Both, the magnetic field  $B$  and spatial gradient  $\partial B/\partial x$  are linearly proportional to the current  $I$  circulating the wires, and thus the magnetophoretic force scales quadratically with the applied field,  $F_m \sim B^2$ , as shown in Fig. 1(a). Each coil is fed independently by a function generator (Tektronix AFG 3021C). The particle dynamics are monitored with a stereomicroscope (Leica Z6 APO) equipped with a  $\times 5$  objective, which allows a magnification of  $\times 18$  (see Video S1 in the Supplemental Material [48]), and a high-speed camera (Photron MiniAx). Image quality is improved via additional back illumination of the sample plane.

Our colloidal system consists of carbonyl iron particles (Merck) with mean diameter of  $d \sim 4$   $\mu\text{m}$  and a density of  $\rho = 7.8$  g cm $^{-3}$ , which is higher than the dispersing medium. Thus, once dispersed in a solution, the particles sediment close to the bottom of the experimental cell. Under the action of an external field  $\mathbf{B}$ , and assuming a point dipole approximation, the particle moment is given by  $\mathbf{m} = d^3 \pi K \mathbf{B} / (2\mu_0)$ , with  $K = (\mu_p - \mu_0) / (\mu_p + 2\mu_0) \sim 0.65$  being the Clausius-Mosotti factor and  $\mu_p$  and  $\mu_0$  the magnetic permeability of the particle and the medium, respectively. Thus, a magnetic gradient  $\nabla \mathbf{B}$  exerts a net force  $\mathbf{F}_m = (d^3 \pi K) / (2\mu_0) \mathbf{B} \cdot \nabla \mathbf{B}$  directed along the strongest magnetic field intensity for  $K > 0$ , which corresponds to a positive magnetophoresis.

As an example of a time-independent, non-Newtonian medium we choose to use a power-law fluid, where the viscosity is proportional to some power of the shear rate. Our dispersing medium is a prototypical biopolymer with shear thinning behavior, namely a solution composed of Xanthan gum (Merck) dispersed in highly deionized water (milliQ, Millipore) at 0.025 wt%. From rheological measurements, Fig. 1(b), we find that the Xanthan gum solution presents a strong shear thinning behavior, where the variation in viscosity can be well described by a power-law model in the range of shear rates used,

$$\eta = \kappa \dot{\gamma}^{n-1}, \quad \tau = \kappa \dot{\gamma}^n, \quad (1)$$

with  $\dot{\gamma}$  being the shear rate,  $\tau$  the shear stress,  $\kappa$  the consistency index, and  $n$  the power-law index [49,51]. Equation (1) can also be recovered from the Yasuda-Carreau model for non-Newtonian fluids [52].

Furthermore, this behavior agrees with previous works, which also show that diluted Xanthan gum solutions are relatively inelastic [53]. Moreover, we use three-dimensional numerical simulations in computational fluid dynamics using COMSOL software to confirm the validity of the power-law model [Eq. (1)]. We analyze the shear rate for a 4- $\mu\text{m}$ -diameter particle moving at a speed of  $v = 10 \mu\text{m s}^{-1}$ . As shown in Fig. S1 in [48], for a power-law fluid with  $\kappa = 10^{-2.58} \text{ Pa s}^n$  and  $n = 0.76$ , values of the shear rate as large as  $\dot{\gamma} = 14 \text{ s}^{-1}$  are reached at the particle surface. More details are given in [48].

To apply a periodic driving force so that it induces a zero-mean displacement in a Newtonian fluid, we use the following protocol, also illustrated in Fig. 2(a); see also Video S1 in [48]. We apply a periodic forcing in the form of an asymmetric square wave composed of two plateaus of duration  $T_i$  with  $i = 1, 2$  and a constant period  $T = T_1 + T_2$ . During the first time interval  $T_1$ , we apply a force  $F_1$  along the positive direction ( $x > 0$ ), while during  $T_2$  another force of amplitude  $F_2$  is applied along the opposite direction ( $x < 0$ ). We choose the time periods and force amplitudes so that they are dissimilar, and such that the force difference  $\Delta F = F_1 - F_2 \neq 0$  while the product  $F_1 T_1 = F_2 T_2$  is constant. Thus, in a Newtonian fluid such as water, due to the constant

viscosity and linear relationship between the applied force and the acquired speed, a dispersed magnetic particle will experience a series of cyclic oscillations with a zero-mean velocity  $\bar{v} = 0$  when averaged over several field periods.

Our main results in a shear thinning fluid are shown in Fig. 2(b). For a completely symmetric drive with  $\Delta F = 0$  and  $T_1 = T_2$ , a dispersed particle undergoes a periodic displacement along the driving direction, which consists of triangular oscillations of amplitude  $\Delta x$  and  $\bar{v} = 0$ . However, the situation changes when varying the field parameters ( $F_i, T_i$ ), while keeping constant the product  $F_1 T_1 = F_2 T_2$ . As shown in Fig. 2(b), we observe  $\bar{v} > 0$  for a force difference  $\Delta F > 0$  and  $T_1 < T_2$  and  $\bar{v} < 0$  in the opposite case. In particular, for  $F_1 = 0.84 \text{ pN}$ ,  $F_2 = 0.42 \text{ pN}$ , and  $T_1 = 0.5 T_2$ , the particle motion is characterized by a net speed of  $v = 7.80 \pm 0.11 \mu\text{m s}^{-1}$  for the half-interval  $T_1 = 2 \text{ s}$  and  $v = -3.680 \pm 0.015 \mu\text{m s}^{-1}$  for the second half-interval of duration  $T_2 = 4 \text{ s}$ . This difference induces a positive increment of  $\Delta x = 0.766 \mu\text{m s}^{-1}$  in a period  $T = 6 \text{ s}$  and a final total displacement of  $\sum_i \Delta x_i = 15.6 \mu\text{m s}^{-1}$  after  $N = 15$  periods. Thus, the magnetic particle acquires a positive mean speed of  $\bar{v} = 0.19 \mu\text{m s}^{-1}$ . In contrast, reversing the duration of the two time intervals,  $T_1 = 2 T_2$ , and the force difference,  $\Delta F \rightarrow -\Delta F$ , produces a series of negative displacements leading to an opposite velocity of  $\bar{v} = -0.23 \mu\text{m s}^{-1}$ . We note that applying the same protocol to the particle dispersed in water leads to zero mean velocity, due to the absence of the shear thinning. Also, for very large and small shear rates,  $\dot{\gamma} \rightarrow 0$  and  $\dot{\gamma} \rightarrow \infty$ , shear thinning fluids acquire typically constant viscosity and the ratchet effect vanishes. Thus, our ratchet transport [as Eq. (1)] will work only for intermediate ranges of the shear rate and magnetic forcing. Moreover, a similar protocol was used in [54] to numerically simulate driven particles dispersed in a bath of passive spheres, but this was not in a continuous medium as in this study.

The emergent particle transport is a result of the balance between the applied magnetic force and the viscous dissipation that arises from the net particle motion. The equation of motion for the driven particle can be written as  $m_p \mathbf{a} = \mathbf{F}_m + \mathbf{F}_v$ , with  $m_p$  being the mass of the particle and  $\mathbf{F}_v$  the viscous drag due to the particle motion. Here we neglect thermal fluctuations due to the relatively large particle density and negligible small diffusion coefficient,  $D = 0.0052 \mu\text{m}^2 \text{ s}^{-1}$ , as measured from the mean-square displacement of the particles in a Xanthan gum solution. For an inelastic power-law fluid, the viscous drag force can be written as

$$F_v = \frac{d^2 \pi v^2 \rho C_D}{8}, \quad (2)$$

with  $C_D = 24X/\text{Re}_{pl}$ ,  $\text{Re}_{pl} = \rho v^{2-n} d^n / \kappa$ , and  $X$  a correction factor that is a polynomial function of  $n$  (see later). In the overdamped limit, the equation of motion can be

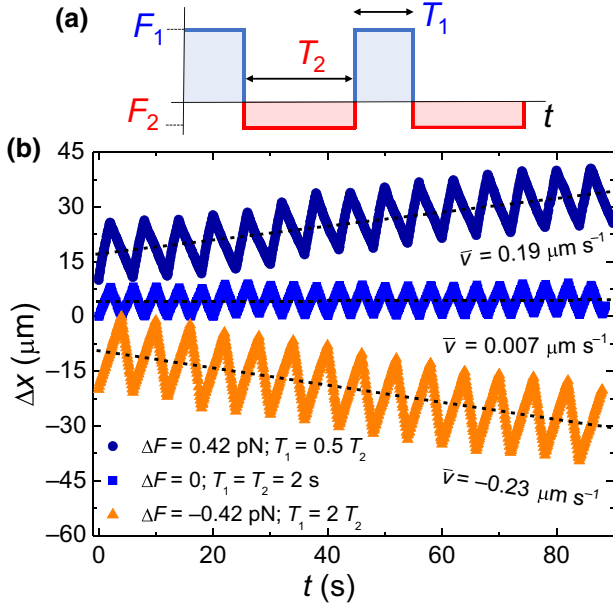


FIG. 2. (a) Schematic illustrating the protocol used to apply the square-wave magnetic forcing. The product of the force amplitudes and lags times is kept constant,  $F_1 T_1 = F_2 T_2$ . (b) Displacement  $\Delta x$  versus time  $t$  of a magnetic particle driven in a Xanthan gum solution under a totally symmetric drive  $F_1 = F_2$  (blue squares), and two asymmetric drives such that  $\Delta F > 0$  (navy disks, upper data) and  $\Delta F < 0$  (orange triangle, lower data). To avoid overlap between the experimental data, the displacement of the upper disks (lower triangles) has been shifted by  $\Delta x = 10 \mu\text{m s}^{-1}$  ( $\Delta x = -20 \mu\text{m s}^{-1}$ ).

exactly solved. Indeed, Eq. (2) can be rewritten as  $F_v = -\gamma_n |v|^n \text{sign}(v)$ , where  $\gamma_n = 3\pi\kappa X d^{2-n}$ , which gives the velocity  $v_{1,2} = (F_{1,2}/\gamma_n)^{1/n} \text{sign}(F_{1,2})$ . From the difference between the displacements in each direction, it follows that  $\bar{v} = v_1 T_1 - v_2 T_2 / T_1 + T_2$ , and given  $F_1 T_1 = F_2 T_2$  we obtain

$$\bar{v} = \frac{1 - (T_1/T_2)^{1/n-1} \left(\frac{F_1}{\gamma_n}\right)^{1/n}}{1 + T_2/T_1} \quad (3)$$

We also numerically integrate the equation of motion under the magnetic force protocol used for both water ( $F_v = 3\pi d \eta v$ , with  $\eta = 10^{-3}$  Pa s) and the power-law fluid, considering also the particle inertia. In the simulation we use  $X = 1.275 + 0.965n - 1.408n^2 + 0.176n^3$  [55]. As further data we use  $\kappa = 10^{-2.58}$  Pa s<sup>*n*</sup> and  $n = 0.76$ , and find similar trajectories to the experimental ones for both cases.

The main results of the model and numerical simulations are shown in Fig. 3 for the Xanthan gum solution. There we report the absolute value of the average speed of the experimental trajectories as a function of the force amplitude during the first time period,  $F_1$ , for time intervals  $T_1 = 4$  s and  $T_2 = 2$  s. Note that, for these values of  $T_{1,2}$ ,  $\bar{v} < 0$ . In the Supplemental Material [48], we show the results from the absolute value of the average speed when varying the period duration  $T_1$  while keeping  $F_1 = 0.3$  pN and  $F_2 = 0.6$  pN constant. Both the model and the simulations predict that the mean velocity raises as a power law of exponent 1.3, as shown in the small inset in Fig. 3, and it agrees qualitatively with the

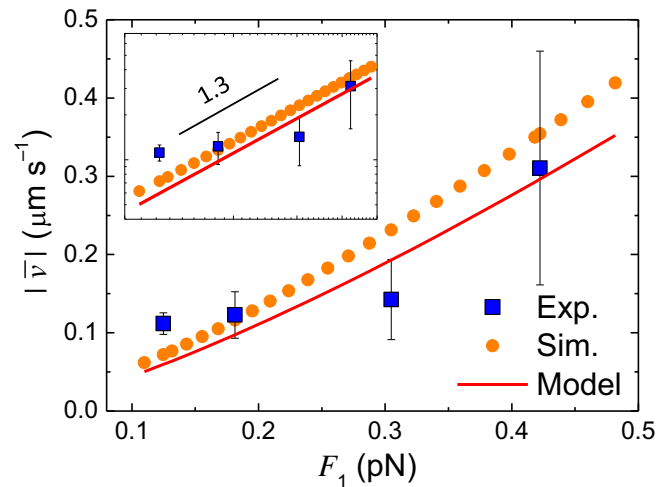


FIG. 3. Absolute value of the mean speed  $|\bar{v}|$  versus first force amplitude  $F_1$  with  $T_1 = 4$  s and  $T_2 = 2$  s. The scattered blue squares are experimental data, the orange disks result from numerical simulations, and the continuous red line is a nonlinear regression of the experimental data using Eq. (3). The small inset at the top shows the log-log plot of the main graph illustrating the slope of a power law of exponent 1.3.

behavior reported from the experimental data, within the corresponding error bars. Such an exponent can be easily justified by using Eq. (2) in the overdamped limit, which predicts that, for  $n = 0.76$ , the applied magnetophoretic force should scale as  $F_m \sim \bar{v}^{0.76}$ ; this gives the observed relationship  $\bar{v} \sim F_m^{1.3}$ , which is valid for both time periods. If we use Eq. (3) to fit the experimental data by keeping  $n = 0.76$  fixed and let  $\gamma_n$  vary, we find that the best match to the data, shown by the continuous red line in Fig. 3, is achieved when the obtained value of  $\gamma_n$  predicts a particle diameter equal to  $d = 6.1 \pm 0.2$   $\mu\text{m}$ . This value is larger than the experimental one ( $d \sim 4$   $\mu\text{m}$ ) and the discrepancy can be due to different reasons. For example, in our model we neglect the hydrodynamic interaction of the particle with the close wall and assume a point dipole approximation when considering the magnetic moment  $m$  induced by the applied field. Further sources of discrepancy could be due to the presence of disorder in the experimental system in the form of a nonuniform particle shape or a different magnetic moment under the applied field. However, we note that, due to the relatively high apparent viscosity of the dispersing medium, the chosen particles represent the best compromise between microscopic size and strong, induced magnetization, allowing their manipulation in the biopolymer matrix.

In conclusion, we have experimentally demonstrated a deterministic ratchet effect in an inelastic shear thinning fluid by using magnetic colloids under a time-dependent, asymmetric square-wave drive. The net particle transport arises from the strong shear thinning behavior of the dispersing medium, which causes a lower viscous dissipation when increasing the magnetic force, in contrast to the behavior observed in a simple Newtonian fluid. Our experimental setup allows the application of forces of the order of piconewtons to magnetizable particles, and thus can be employed to explore the rheological properties of many other complex fluids that are characterized by a relatively large viscosity. Indeed, a natural follow up of this work would be to extend the proposed technique to elastic and time-dependent fluids. Since magnetic microrheology is based on the oscillatory motion of dispersed particles under time-dependent fields [56–59], we believe that our approach could be used to directly measure the complex moduli of viscoelastic fluids. Also, the experimental results of this paper could stimulate further theoretical work on the subject of ratcheting particles in non-Newtonian fluids. For example, we could consider smaller particles and investigate how thermal fluctuations may limit the transport mechanism. The reduction of the friction coefficient in shear thinning fluid may have important consequences for particle diffusion and transport, leading to emergent effects [60,61].

*Acknowledgments.*—We thank an anonymous Referee for useful insights into the theory part. This work was

supported by the ERDF, the FEDER, the MICINN AE Projects No. EQC2019-005529-P and No. PID2019-104883GB-I00, and the Junta de Andalucía Projects No. P18-FR-2465 and No. A-FQM-396-UGR20. G.C. acknowledges support from an FPU20/04357 Fellowship. J.R.M. acknowledges support from an (EF-ST)-H2020-MSCA-IF-2017 (Grant No. 795318) Fellowship. P.T. acknowledges support from the ERC consolidator Grant Enforce (No. 811234) and from the Generalitat de Catalunya (“ICREA Acadèmia”).

- 
- [1] R. P. Feynman, R. B. Leighton, and M. Sands, *The Feynman Lectures on Physics* Vol. I (Addison-Wesley, Reading, MA, 1966).
- [2] P. Reimann, Brownian motors: noisy transport far from equilibrium, *Phys. Rep.* **361**, 57 (2002).
- [3] P. Hänggi and F. Marchesoni, Artificial Brownian motors: controlling transport on the nanoscale, *Rev. Mod. Phys.* **81**, 387 (2009).
- [4] H. Mazal, M. Iljina, I. Riven, and G. Haran, Ultrafast pore-loop dynamics in a aaa+ machine point to a Brownian-ratchet mechanism for protein translocation, *Sci. Adv.* **7**, eabg4674 (2021).
- [5] R. D. Astumian, Thermodynamics and kinetics of a Brownian motor, *Science* **276**, 917 (1997).
- [6] D. Keller and C. Bustamante, The mechanochemistry of molecular motors, *Biophys. J.* **78**, 541 (2000).
- [7] Y. Nakayama and S. Toyabe, Optimal Rectification Without Forward-Current Suppression By Biological Molecular Motor, *Phys. Rev. Lett.* **126**, 208101 (2021).
- [8] J. W. McCausland, X. Yang, G. R. Squyres, Z. Lyu, K. E. Bruce, M. M. Lamanna, B. Söderström, E. C. Garner, M. E. Winkler, J. Xiao, and J. Liu, Treadmilling FtsZ polymers drive the directional movement of spg-synthesis enzymes via a Brownian ratchet mechanism., *Nat. Commun.* **12**, 609 (2021).
- [9] S. Deffner and C. Jarzynski, Information Processing and the Second Law of Thermodynamics: An Inclusive, Hamiltonian Approach, *Phys. Rev. X* **3**, 041003 (2013).
- [10] P. Strasberg, G. Schaller, T. Brandes, and M. Esposito, Quantum and Information Thermodynamics: A Unifying Framework Based on Repeated Interactions, *Phys. Rev. X* **7**, 021003 (2017).
- [11] A. Kolchinsky and D. H. Wolpert, Work, Entropy Production, and Thermodynamics of Information Under Protocol Constraints, *Phys. Rev. X* **11**, 041024 (2021).
- [12] J. M. R. Parrondo, G. P. Harmer, and D. Abbott, New Paradoxical Games Based on Brownian Ratchets, *Phys. Rev. Lett.* **85**, 5226 (2000).
- [13] J.-P. Bouchaud, A. Matacz, and M. Potters, Leverage Effect in Financial Markets: The Retarded Volatility Model, *Phys. Rev. Lett.* **87**, 228701 (2001).
- [14] K. Kanazawa, T. Sueshige, H. Takayasu, and M. Takayasu, and Derivation of the Boltzmann Equation for Financial Brownian Motion: Direct Observation of the Collective Motion of High-Frequency Traders, *Phys. Rev. Lett.* **120**, 138301 (2018).
- [15] Y.-f. He, B.-q. Ai, C.-x. Dai, C. Song, R.-q. Wang, W.-t. Sun, F.-c. Liu, and Y. Feng, Experimental Demonstration of a Dusty Plasma Ratchet Rectification and its Reversal, *Phys. Rev. Lett.* **124**, 075001 (2020).
- [16] M. J. Skaug, C. Schwemmer, S. Fringes, C. D. Rawlings, and A. W. Knoll, Nanofluidic rocking Brownian motors, *Science* **359**, 1505 (2018).
- [17] R. L. Stoop, A. V. Straube, and P. Tierno, Enhancing nanoparticle diffusion on a unidirectional domain wall magnetic ratchet, *Nano Lett.* **19**, 433 (2018).
- [18] A. Libál, C. Nisoli, C. Reichhardt, and C. J. Reichhardt, Dynamic control of topological defects in artificial colloidal ice, *Sci. Rep.* **7**, 651 (2017).
- [19] S. Gliga, G. Hrkac, C. Donnelly, J. Büchi, A. Kleibert, J. Cui, A. Farhan, E. Kirk, R. V. Chopdekar, Y. Masaki, N. S. Bingham, A. Scholl, R. L. Stamps, and L. J. Heyderman, Emergent dynamic chirality in a thermally driven artificial spin ratchet, *Nat. Mater.* **16**, 1106 (2017).
- [20] A. Pérez-Junquera, V. I. Marconi, A. B. Kolton, L. M. Álvarez-Prado, Y. Souche, A. Alija, M. Vélez, J. V. Anguita, J. M. Alameda, J. I. Martín, and J. M. R. Parrondo, Crossed-Ratchet Effects for Magnetic Domain Wall Motion, *Phys. Rev. Lett.* **100**, 037203 (2008).
- [21] J. H. Franken, H. J. M. Swagten, and B. Koopmans, Shift registers based on magnetic domain wall ratchets with perpendicular anisotropy, *Nat. Nano* **7**, 499 (2012).
- [22] M. B. Hastings, C. J. O. Reichhardt, and C. Reichhardt, Ratchet Cellular Automata, *Phys. Rev. Lett.* **90**, 247004 (2003).
- [23] J. E. Villegas, S. Savelev, F. Nori, E. M. Gonzalez, J. V. A. R. Garcia, and J. L. Vicent, A superconducting reversible rectifier that controls the motion of magnetic flux quanta, *Science* **302**, 1188 (2003).
- [24] C. C. de Souza Silva, J. V. de Vondel, M. Morelle, and V. V. Moshchalkov, Controlled multiple reversals of a ratchet effect, *Nature* **440**, 651 (2006).
- [25] P. Galajda, J. Keymer, P. Chaikin, and R. Austin, A wall of funnels concentrates swimming bacteria, *J. Bacteriol.* **189**, 8704 (2007).
- [26] L. Angelani, R. Di Leonardo, and G. Ruocco, Self-Starting Micromotors in a Bacterial Bath, *Phys. Rev. Lett.* **102**, 048104 (2009).
- [27] R. D. Leonardo, L. Angelani, D. Dell’Arciprete, G. Ruocco, V. Iebba, S. Schippa, M. P. Conte, F. Mecarini, F. D. Angelis, and E. D. Fabrizio, Bacterial ratchet motors, *Proc. Nat. Acad. Sci. U.S.A.* **107**, 9541 (2010).
- [28] C. J. O. Reichhardt and C. Reichhardt, Ratchet effects in active matter systems, *Ann. Rev. Cond. Matt. Phys.* **8**, 51 (2017).
- [29] C. Marquet, A. Buguin, L. Talini, and P. Silberzan, Rectified Motion of Colloids in Asymmetrically Structured Channels, *Phys. Rev. Lett.* **88**, 168301 (2002).
- [30] B. B. Yellen, O. Hovorka, and G. Friedman, Arranging matter by magnetic nanoparticle assemblers, *Proc. Nat. Acad. Sci. U.S.A.* **102**, 8860 (2005).
- [31] A. Ros, R. Eichhorn, J. Regtmeier, T. T. Duong, P. Reimann, and D. Anselmetti, Absolute negative particle mobility, *Nature* **436**, 928 (2005).

- [32] S.-H. Lee, K. Ladavac, M. Polin, and D. G. Grier, Observation of Flux Reversal in a Symmetric Optical Thermal Ratchet, *Phys. Rev. Lett.* **94**, 110601 (2005).
- [33] P. Tierno and T. M. Fischer, Excluded Volume Causes Integer and Fractional Plateaus in Colloidal Ratchet Currents, *Phys. Rev. Lett.* **112**, 048302 (2014).
- [34] A. V. Arzola, M. Villasante-Barahona, K. Volke-Sepúlveda, P. Jákl, and P. Zemánek, Omnidirectional Transport in Fully Reconfigurable Two Dimensional Optical Ratchets, *Phys. Rev. Lett.* **118**, 138002 (2017).
- [35] J. R. Gomez-Solano, A. Blokhuis, and C. Bechinger, Dynamics of Self-Propelled Janus Particles in Viscoelastic Fluids, *Phys. Rev. Lett.* **116**, 138301 (2016).
- [36] N. Narinder, C. Bechinger, and J. R. Gomez-Solano, Memory-Induced Transition from a Persistent Random Walk to Circular Motion for Achiral Microswimmers, *Phys. Rev. Lett.* **121**, 078003 (2018).
- [37] K. Qi, E. Westphal, G. Gompper, and R. G. Winkler, Enhanced Rotational Motion of Spherical Squirmer in Polymer Solutions, *Phys. Rev. Lett.* **124**, 068001 (2020).
- [38] I. Goychuk, Subdiffusive Brownian ratchets rocked by a periodic force, *Chem. Phys.* **375**, 450 (2010).
- [39] I. Goychuk and V. Kharchenko, Fractional Brownian motors and stochastic resonance, *Phys. Rev. E* **85**, 051131 (2012).
- [40] I. Goychuk, Viscoelastic subdiffusion: generalized Langevin equation approach, *Adv. Chem. Phys.* **150**, 187 (2012).
- [41] V. Kharchenko and I. Goychuk, Flashing subdiffusive ratchets in viscoelastic media, *New J. Phys.* **14**, 043042 (2012).
- [42] V. O. Kharchenko and I. Goychuk, Subdiffusive rocking ratchets in viscoelastic media: transport optimization and thermodynamic efficiency in overdamped regime, *Phys. Rev. E* **87**, 052119 (2013).
- [43] I. Goychuk, V. O. Kharchenko, and R. Metzler, How molecular motors work in the crowded environment of living cells: coexistence and efficiency of normal and anomalous transport, *PLoS ONE* **9**, e91700 (2014).
- [44] I. Goychuk, V. O. Kharchenko, and R. Metzler, Molecular motors pulling cargos in the viscoelastic cytosol: how power strokes beat subdiffusion, *Phys. Chem. Chem. Phys.* **16**, 16524 (2014).
- [45] I. Goychuk, Anomalous transport of subdiffusing cargos by single kinesin motors: the role of mechano-chemical coupling and anharmonicity of tether, *Biosystems* **12**, 016013 (2015).
- [46] I. Goychuk, Molecular machines operating on the nanoscale: from classical to quantum, *Beilstein J. Nanotechnol.* **7**, 328 (2016).
- [47] I. Goychuk, Perfect anomalous transport of subdiffusive cargos by molecular motors in viscoelastic cytosol, *Phys. Biol.* **177**, 56 (2019).
- [48] See Supplemental Material at <http://link.aps.org/supplemental/10.1103/PhysRevApplied.19.L021001> for additional details on the experimental system and one video illustrating the particle dynamics.
- [49] G. Cuvelier and B. Launay, Concentration regimes in Xanthan gum solutions deduced from flow and viscoelastic properties, *Carbohydrate Polym.* **6**, 321 (1986).
- [50] J. de Vicente, J. R. Stokes, and H. A. Spikes, Soft lubrication of model hydrocolloids, *Food Hydrocoll.* **20**, 483 (2006).
- [51] M. M. Mrokowska and A. Krztoń-Maziopa, Viscoelastic and shear-thinning effects of aqueous exopolymer solution on disk and sphere settling, *Sci. Rep.* **9**, 7897 (2019).
- [52] K. Yasuda, R. C. Armstrong, and R. E. Cohen, Shear flow properties of concentrated solutions of linear and star branched polystyrenes, *Rheol. Acta* **20**, 163 (1986).
- [53] P. E. Arratia, G. A. Voth, and J. P. Gollub, Stretching and mixing of non-Newtonian fluids in time-periodic flows, *Phys. Fluids* **17**, 053102 (2005).
- [54] C. Reichhardt, C. J. O. Reichhardt, and M. B. Hastings, Glassy ratchets for collectively interacting particles, *Phys. Lett. A* **342**, 162 (2005).
- [55] R. P. Chhabra, *Bubbles, Drops, and Particles in Non-Newtonian Fluids* (CRC Press, Boca Raton, 2007), 2nd ed.
- [56] A. R. Bausch, F. Ziemann, A. A. Boulbitch, K. Jacobson, and E. Sackmann, Local measurements of viscoelastic parameters of adherent cell surfaces by magnetic bead microrheometry, *Biophys. J* **75**, 2038 (1998).
- [57] C. Gosse and V. Croquette, Magnetic tweezers: micromanipulation and force measurement at the molecular level, *Biophys. J* **82**, 3314 (2002).
- [58] K. C. Neuman and A. Nagy, Local measurements of viscoelastic parameters of adherent cell surfaces by magnetic bead microrheometry, *Nat. Methods* **5**, 491 (2008).
- [59] L. Chevry, N. K. Sampathkumar, A. Cebers, and J.-F. Berret, Magnetic wire-based sensors for the microrheology of complex fluids, *Phys. Rev. E* **88**, 062306 (2013).
- [60] I. Goychuk and T. Pöschel, Nonequilibrium Phase Transition to Anomalous Diffusion and Transport in a Basic Model of Nonlinear Brownian Motion, *Phys. Rev. Lett.* **127**, 110601 (2021).
- [61] I. Goychuk, Resonance-like enhancement of forced nonlinear diffusion as a nonequilibrium phase transition, *New J. Phys.* **24**, 043018 (2022).